Modelling Water Droplet Movement on a Leaf Surface

MOA'ATH N. OQIELAT*,[a], IAN W. TURNER[a], JOHN A. BELWARD[a], SCOTT W. MCCUE[a]

[a] *Mathematical Sciences, Queensland University of Technology, GPO Box 2434, Brisbane, Queensland 4001, Australia.*

Abstract

Modelling droplet movement on leaf surfaces is an important component in understanding how water, pesticide or nutrient is absorbed through the leaf surface. A simple mathematical model is proposed in this paper for generating a realistic, or natural looking trajectory of a water droplet traversing a virtual leaf surface. The virtual surface is comprised of a triangular mesh structure over which a hybrid Clough-Tocher seamed element interpolant is constructed from real-life scattered data captured by a laser scanner. The motion of the droplet is assumed to be affected by gravitational, frictional and surface resistance forces and the innovation of our approach is the use of thin-film theory to develop a stopping criterion for the droplet as it moves on the surface. The droplet model is verified and calibrated using experimental measurement; the results are promising and appear to capture reality quite well.

Key words: Mathematical modelling, Surface fitting, thin-film approximation, Clough-Tocher method, radial basis function method.

1. Introduction

An important research component of agrichemical spray retention by plants is to model and simulate droplet movement on the surface of a leaf. To this end, we present a simple mathematical model for this process, report on experimental results generated with a particular type of leaf (Frangipani

*Corresponding author: i.turner@qut.edu.au, Tel.: +61 7 3138 2259

leaf), and compare the results from each of the two studies. A crucial aspect of our approach is to construct the surface of the leaf using a recently developed surface fitting method [28, 29] based on a combination of the Clough-Tocher method with radial basis functions.

When a single water droplet impacts on a solid surface, it may bounce off or perhaps spread out along that surface, depending on the nature and inclination of the surface, the speed and size of the drop, and the properties of the liquid, including the viscosity and surface tension. However, in reality there are more options for the fate of the droplet, and indeed Rioboo et al. [41] report that their experiments suggest the outcomes include deposition, prompt splash, corona splash, receding break-up, partial rebound, and complete rebound. These are also described qualitatively in the review article by Yarin [42]. Further, spreading drops may be characterised by instabilities leading to viscous fingering, as studied by Kim et al. [39] and Thoroddsen and Sakakibara [40], for example. An important point is that the detailed fluid mechanics of each of these outcomes is quite sophisticated, and requires high level mathematical modelling, including asymptotic and stability analysis and careful computational simulations, as well as an expensive experimental setup.

At present none of these ideas has been included in mathematical models for droplet impaction and/or spreading on leaf surfaces. While these issues may be addressed in further research, the purpose of the present study is to develop a simplified model based in part on previous studies on droplet movement, in order to provide, for the first time, a realistic simulation of droplet movement on leaf surfaces. The gravity-driven model is effectively one-dimensional, with droplet movement described as a polygonal path of curved arcs. A novel feature of this approach is that a thin-film model is used to develop a stopping criterion for the droplet. Experimental verification of the droplet model shows that it captures reality quite well and produces realistic droplet motion on the leaf surface. Most importantly, it is observed that the simulated droplet motion follows the contours of the surface and stops moving at times consistent with experimental observation (see figure 9, for example).

While this research makes its contribution through simulation and visualisation of the realistic movement of a water droplet flowing on a leaf surface, we do not address certain, possibly important, phenomena such as the effect that the microscopic detail of each different variety of leaf surface has on the droplet motion. Further, we do not attempt to describe the time-dependent

shape of each droplet via the Navier-Stokes equations, and as such we do not model the actual droplet motion in any realistic way from a fluid mechanics perspective. We remark, however, that our simplified model is able to produce quite realistic droplet motion and is the most inclusive of any that have appeared to date.

In order to simulate water droplet movement on the leaf surface, the "virtual" surface itself needs to be constructed using surface fitting methods. Loch [22] uses two such approaches based on the finite element method to model the leaf surface. In earlier work [28, 29] we introduced a new surface fitting method based on hybrid strategies that combine the Clough-Tocher method [20, 4] with radial basis functions [13, 33] for this purpose. This method is based on a large number of three-dimensional data points captured from an actual leaf surface using a laser scanner. To apply the hybrid method to the leaf data sets, preprocessing steps are required, which include the determination of a reference plane for the data and the subsequent triangulation for the leaf surface mesh [28, 29]. In this paper, the hybrid method is used to construct the surface of a Frangipani leaf for the purpose of simulating water droplet movement on that surface.

The outline of the paper is as follows. In §2 a relevant literature review of droplet simulation is presented. A brief description of the leaf surface model is explained in §3. In §4 an overview of the droplet model is presented. Two forces are assumed to affect the droplet movement on the leaf surface namely an internal force, which consists of a friction and resistance component between the surface and the droplet, and an external force due to gravity. The surface is divided into a mesh of triangles [28, 29] and the motion of the droplet is computed over each triangle. The inclusion of a thin-film concept enables the motion of the droplet to be stopped at a point where the height of the thin-film along the polygonal path is less than some specified tolerance. As a result, we observe using our model that if the leaf surface is horizontal, or close to horizontal, the droplet moves along the leaf vein; on other occasions the droplet moves and then falls from the surface. The model also shows that the droplet stops moving on the surface or it leaves the surface depending on the model parameters. In §5, an experimental verification of the water droplet model for a Frangipani leaf is presented. Finally, the work is concluded in §6, where future work and other applications of our research are discussed.

2. Relevant Literature and Experiments

Several researchers have studied the animation of water droplets since the 1980's [8, 9, 11, 30]. However, only a limited number of methods, during the 1990's, address the natural phenomenon of water droplets flowing on surfaces where, typically, meta-balls in a gravitational field were used [35] to model static droplet shapes on flat surfaces. Tong et al. [34] modelled water flows using meta-balls by proposing a volume-preserving approach. Lanfen [21] presented a physical model for two, or more, large water droplets morphing on a plane. Kaneda et al. [16] proposed a method for generating an animation of water droplets and streams on a glass plate (divided into a small mesh composed of quadrilateral elements), such as a windowpane or windshield. This model takes into account the dominant parameters of the dynamical system, which include gravity, interfacial tensions and the collision of droplets. To every lattice point on the glass plate, an affinity for water ($0 \leq c_{i,j} \leq 1$) is assigned in advance. A sphere was used to model the droplet on a plate.

The method in [16] is not able to simulate flow of a droplet on a curved surface. Kaneda et al. [18] proposed an extended method for generating a realistic animation of water droplets as well as their streams on curved surfaces. The motion of water droplets on the surface depends on the external forces due to gravity and wind and an internal force due to resistance. The droplet flows on the surface and some amount of water remains behind because of the wetting, and later the water flow merges with the remaining water. Therefore a solution to the wetting phenomenon and the problem with two droplets merging is also addressed. Kaneda et al. [17] proposed a method for generating realistic animations of water droplets that meander down a transparent surface based on the work presented in [16, 18]. This work is useful for applications such as drive simulators and animation of water droplets on a windshield. The main difference between this work and previous work is the modelling of obstacles that move against water droplets on a surface, for example a windshield wiper. The droplet is represented by a single particle system and modelled as a sphere. The contact angle between the droplet and the surface is also taken into account.

Jonsson [15] proposed a physically plausible model using normals of the bump map surface in the computation of water droplet flow based on the model presented in [16]. Solid spheres are used to model the droplets, where each droplet is a particle system. Jonsson assumed that the external force

that affects the water droplet flow is due to gravity, while the internal force is due to the resistance. The direction of the internal force is opposite the direction of movement and is computed by applying the Gram Schmidt orthogonalization algorithm [26] to orthogonalise the external force against the unit length normal vector, which is retrieved at every point from the bump map.

Fournier et al. [10] presented a model oriented towards an efficient and visually-satisfying simulation of a droplet moving down a surface. The efficiency arises from the separation between the shape and the motion of the droplet. The aim was to simulate the shape and motion of large liquid droplets travelling down a surface when it is affected by surface roughness, adhesion, gravity and friction forces. The surface is defined by a mesh of triangles. A "neighbourhood" graph is built at the beginning of the simulation so that each triangle is linked to adjacent triangles. The neighbourhood graph is used to identify to which triangle the droplet moves and during the simulation it is known exactly in which triangle a droplet is located. A droplet might traverse several triangles between two time steps. The motion is computed over each individual triangle to ensure the droplet is properly affected by the deviations on the surface it has traversed. The gravity and friction forces are assumed to be constant over a triangle for simplicity, and the friction force is modelled as a linear viscous force with a constant negative factor due to surface roughness. The shape of a droplet is characterized by a small set of properties, for example, volume conservation and surface tension. A droplet will fall from the surface if the component of the droplet acceleration force that is normal to the surface is larger than the adhesion force of the droplet. The motion of the droplet is generated by a particle system, with the droplet represented by a single particle [31].

Computational fluid dynamics has been successfully applied to simulate realistic animation of fluids. Chen [3] presented a disturbance model to simulate water flow using the Navier-Stokes equations. Foster [9, 8] and Enright [5] used this approach to develop liquid surfaces and to simulate complex liquid motion. Losasson [23] simulated water on a refined grid, such as an octree structure instead of a regular grid to capture more surface details using the Navier-Stokes equations. In the model presented in this paper we chose not to use this approach to calculate the motion of the droplet because of the computation expense of this method, which would require solution on each element in the leaf surface mesh.

3. Leaf surface model

As mentioned above, before any simulation of the water droplet movement on a leaf surface can be simulated, it is necessary to construct a "virtual" leaf surface. In previous work by the authors [28, 29] we have introduced a new surface fitting interpolation method that combines the Clough-Tocher method with radial basis functions for this purpose. A set of representative data points sampled from a Frangipani leaf using a laser scanner was used to reconstruct the surface of the leaf. The surface fitting method was then applied to the laser scanned leaf data points to reconstruct the surface. However, in order to apply this method to the leaf data a preprocessing phase was required, which includes the determination of a new reference plane for the data and the subsequent triangulation for the leaf surface mesh.

3.1. Leaf reference plane

The laser scanner returns the coordinates of points on the leaf surface. These coordinates may not necessarily coincide with the xy-plane in the data point coordinate system. To overcome this problem, we used a reference plane that is a least squares fit to these data points and then the coordinate system was rotated so that the reference plane becomes the xy-plane. These rotations can be achieved by at first rotating the normal vector of the reference plane about the y-axis into the yz-plane and then rotating about the x-axis into the xz-plane [28, 29].

3.2. Triangulation of the leaf surface

Our surface fitting method is an interpolation based finite element method and consequently, a triangulation of the leaf surface needs to be constructed. The leaf data points that represent the surface are numerous. As a consequence, a subset of the data set is selected to reduce the computational expense for surface fitting, which is then used to generate the triangulation. This triangulation is generated using the EasyMesh mesh generator, which is software written in the C language by Bojan [25]. EasyMesh generates two-dimensional Delaunay triangulations in general domains. For more details see Oqielat et al. [28, 29]. An example of a triangulated leaf surface is shown in figure 10(c,d).

4. Droplet model

The fundamental unit of the model is a triangular element. We now address the issues of forces on the droplet, a mathematical description of the thin film and the kinematics of the motion. The triangulation offers many advantages; for example, the motion and the position of the droplet over each individual triangle are easy to compute, and the determination of the location of the droplet on the surface at any time instant is straightforward. Such simulations of droplet movement could be computationally demanding if thousands of triangles have to be considered, so a coarser mesh based on a smaller subset of data points is used that is representative of the major surface features (see figure 10 (c-f)).

4.1. External and internal forces

We consider in our model that the external force f^{ext} that affects the droplet movement is due to gravity F_g, which does not change over a triangle. The gravitational force is resolved (projected) in the direction of movement (see figure 1) as

$$d_p = F_g - (F_g \cdot N)N, \tag{1}$$

where N is the unit normal vector and $\{N, d_p/\|d_p\|\}$ is an orthonormal set of vectors. The unit normal vector of the surface is found by letting $S =$

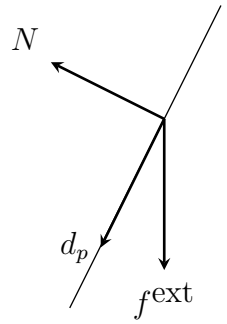

Figure 1: The direction of movement d_p with normal N and gravity f^{ext}.

$(x, y, f(x, y))^T$ be the surface of interest, with tangent vectors $S_x = (1, 0, f_x)^T$ and $S_y = (0, 1, f_y)^T$. The normal of the surface is then given by $n = S_x \times S_y = -f_x i - f_y j + k$, and the unit normal vector $N = n/\|n\|$ is

$$N = \frac{(-f_x, -f_y, 1)}{\sqrt{f_x^2 + f_y^2 + 1}}. \tag{2}$$

The internal force f^{int} consists of a resistance force F_r and a friction, or drag force, F_f. We have adopted the same notation of vectors used by Kaneda et al. [18], Fournier et al. [10] and Jonsson [15] along with the new vectors denoting the gravitational force F_g, the triangle edge $\ell = (\ell_x, \ell_y, \ell_z)^T$, and the droplet position $p = (p_x, p_y, p_z)^T$. The resistance force originates from the interfacial tension that exists between the water droplets and the leaf surface [18, 15], and its direction is opposite to the direction of movement (d_p). This force is modelled using the degree of affinity as

$$F_r = -\alpha d_p,$$

where $0 \leq \alpha \leq 1$ is the affinity, which is set experimentally in advance and assumed to be constant over each triangle. The degree of affinity depends on the interfacial tension as it expresses the status of the surface, such as impurities and small scratches [18]. The friction force F_f is modelled as a linear retarding force with a constant negative factor k_f due to surface roughness [10]:

$$F_f(t) = -k_f v(t),$$

where k_f is the friction coefficient and $v(t)$ is the droplet velocity at time t. The motion of the water droplet on the surface depends on the external force f^{ext}. When this force exceeds a static critical force (internal force f^{int}), the water droplet starts to meander down the surface.

4.2. Thin-film flow down a slope

Although there is a large literature on modelling the spreading of droplets on surfaces, a literature search of papers that describe the simulation of droplet motion on leaf surfaces has found an absence of thin-film theoretic models to approximate when to stop the droplet motion. The one-dimensional flow of a thin-film of viscous fluid down a slope of angle α to the horizontal is governed by the following partial differential equation [19, 24, 27]:

$$\frac{\partial h}{\partial t} + \Big(\frac{g \sin\alpha}{\nu}\Big) h^2 \frac{\partial h}{\partial x} = \frac{\partial}{\partial x}\Big\{\frac{1}{3} h^3 \Big(\frac{g \cos\alpha}{\nu}\frac{\partial h}{\partial x} - \frac{\sigma}{\nu}\frac{\partial^3 h}{\partial x^3}\Big)\Big\}, \tag{3}$$

where $z = h(x,t)$ describes the film height, the x-axis points down the slope, and t is time (see figure 2). The physical parameters that describe the fluid are the kinematic viscosity ν and the surface tension σ. The constant g is the

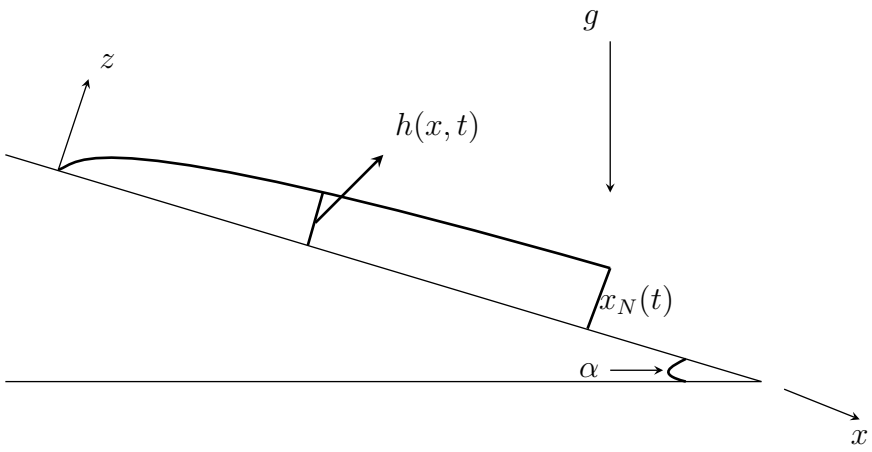

Figure 2: Thin-film flow down a slope.

acceleration due to gravity. Equation (3) is derived under the assumption that the film is 'thin' (a representative height of the fluid h is much less than a typical length L in the x-direction) and the flow is slow (the Reynolds number $\mathrm{Re} = vL/\nu \ll 1$, where v is the velocity scale $v = gh^2/\nu$). Unless the surface of the leaf is horizontal (or nearly horizontal), then away from the front of the film (the nose) equation (3) can be approximated by

$$\frac{\partial h}{\partial t} + \Big(\frac{g \sin\alpha}{\nu}\Big) h^2 \frac{\partial h}{\partial x} = 0. \tag{4}$$

By applying the method of characteristics, the general solution of (4) is found to be

$$h = f\Big(x - \frac{g \sin\alpha}{\nu} h^2 t\Big), \tag{5}$$

where $h(x, 0) = f(x)$ is a function describing the initial profile of the film [1]. Thus, we have a travelling wave type solution with wave speed $gh^2 \sin\alpha/\nu$.

For an initial droplet profile with compact support as shown in figure 2, we can denote the nose of the film by $x_N(t)$, so that at any time t the film is in contact with the substrate in the region $0 < x < x_N(t)$. The x-axis points down the line of steepest descent, which is assumed to be slowly varying per unit distance. As time evolves the profile near the nose of the droplet will steepen, so that surface tension becomes important [14]. However, at intermediate to long times, the height of the main part of the droplet is

small, and in fact, $h \to 0$ as $t \to \infty$. Thus, from (5), we have that [14]

$$h \sim \Big(\frac{\nu}{g \sin \alpha}\Big) \frac{x^{\frac{1}{2}}}{t^{\frac{1}{2}}}, \tag{6}$$

for large times (away from the nose), regardless of the initial profile $f(x)$. By coupling conservation of mass with (6) we can derive the location of the droplet front [14] as

$$x_N(t) = \Big(\frac{9Ag \sin \alpha}{4\nu}\Big)^{\frac{1}{3}} t^{\frac{1}{3}}, \tag{7}$$

where A is the surface area of the thin-film given by

$$A = \int_0^{x_N(t)} h(x,t) dx,$$

and $\sin \alpha$ is computed as

$$\sin \alpha = \frac{F_g \cdot d_p}{\|F_g\| \|d_p\|},$$

where d_p is the direction of movement given by (1).

As mentioned before, the leaf surface is represented by a mesh of triangles across which the droplet moves. To implement the thin-film concept in our model, we compute the height of the thin-film given in equation (6) over the known (computed) droplet path on each triangle to determine the height of the thin-film along its polygonal path. If this height is less than a set tolerance ϵ the droplet movement is stopped, otherwise it will continue to move to the triangle edge. More details on this algorithm are given in the next section.

4.3. Motion of a droplet over the leaf surface

We first develop a single droplet model. It offers many advantages in terms of flexibility and generality; for instance, it will make the droplet movement straightforward to control and it will be easy to add more droplets to the animation at a later stage.

Newton's second law $F = ma$ is used to determine the features of the motion, so that the droplet is specified according to position p, acceleration a, velocity v and mass m. The forces acting on the droplet movement (given in section 4.1) are then taken into consideration to derive the model:

$$m\frac{dv}{dt} = md_p - k_f v(t) - \alpha d_p, \tag{8}$$

where αd_p is the resistance force and $k_f v(t)$ is the frictional force due to air. One way to estimate the parameter k_f is to use Stokes's law for a resistance for a sphere moving through air of radius $r = 0.001(\text{m})$, which has the same volume as the droplet used in our simulations, to give $k_f v \sim O(10^{-8})(kg.m/s^2)$. The mass m of the droplet is assumed to be constant.

In our model, the droplet moves down the virtual leaf surface defined as a mesh of triangles, which offers the benefit in that the equation of motion is simplified for an individual triangle.
At the beginning of the simulation, a droplet rolls on the virtual leaf structure. We specify the initial time t_0, the initial velocity v_0, initial position p_0, the transit time of the droplet, which is accumulated as the droplet moves from one triangle to another and the time frame (total specified transit time). We determine the initial triangle from which the droplet commences to move using the Matlab command tsearch. Next, we determine the direction of movement using equation (1) and then allow the droplet to move to the next triangle. The time taken for the droplet to move to the next element is calculated and the accumulated transit time is stored.

Suppose that the droplet enters the k^{th} triangle at time $t = t_k$ (see figure 3). The velocity and the position of the droplet are then computed respectively using equations (9) and (10). Denote the droplet transit time for the k^{th} triangle as t_f. The time interval $[t_k, t_k + t_f]$ is discretised into N_t divisions using $\Delta t = t_f/N_t$ for the purposes of calculating the thin-film height and visualising the droplet motion. As the droplet traces a path across the triangle it can be located on the leaf surface at the time instant $t_d = t_k + i\Delta t$, $i = 1, \cdots, N_t$ using $p(t_d)$. Next, the location of the droplet front $x_N(t_d)$ is

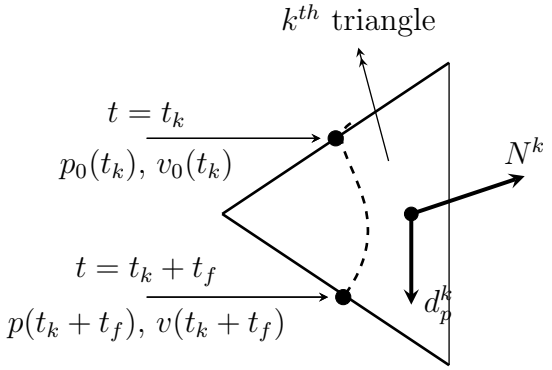

Figure 3: The droplet movement within the k^{th} triangle.

computed using equation (7). The height of the thin-film h is evaluated by substituting $x_N(t_d)$ into equation (6). Finally, the droplet is moved to the next triangle provided the accumulated transit time is less than the time frame and the height of the thin-film is above a specified tolerance, here taken as $h > \epsilon = 10^{-5}m$.
The motion of the droplet is computed over each triangle and the equation for velocity and position of the water droplet at any time t are derived from equation (8) as follows:

$$v(t) = -\frac{m}{k_f}\overline{d_p^k} + \Big(\frac{m}{k_f}\overline{d_p^k} + v_0(t_k)\Big)\exp(tk_f/m), \tag{9}$$

$$p(t) = p_0(t_k) - \Big(\frac{m}{k_f}\overline{d_p^k}\Big)t + \frac{m}{k_f}\Big(\frac{m}{k_f}\overline{d_p^k} + v_0(t_k)\Big)\Big\{\exp(tk_f/m) - 1\Big\}, \tag{10}$$

where $v_0(t_k)$, $p_0(t_k)$ and d_p^k are respectively the initial velocity, the initial position and the direction of movement of the droplet at the time t_k when it enters the k^{th} triangle, see figure 3, and we have defined $\overline{d_p^k} = (1 - \alpha/m)d_p^k$. When the droplet enters the k^{th} triangle at time t_k, we directly computed the transit time t_f, the exit time $t_d = t_k + t_f$ and the exit position $p(t_d)$ as well as the velocity $v(t_d)$ at this time, the transit time t_f is found by intersecting the droplet path using equation (10) with each triangle edge using a Newton algorithm. We now explain this strategy in the following paragraphs.

Each triangle edge has three components $(\ell_x, \ell_y, \ell_z)^T$ that are given in standard parametric form by:

$$\begin{aligned}
\ell_x(\tau) &= a_{ix} + \tau(a_{jx} - a_{ix}),\\
\ell_y(\tau) &= a_{iy} + \tau(a_{jy} - a_{iy}),\\
\ell_z(\tau) &= a_{iz} + \tau(a_{jz} - a_{iz}),
\end{aligned}$$

where the parameter $0 \le \tau \le 1$, $(a_{ix}, a_{iy}, a_{iz})^T$ and $(a_{jx}, a_{jy}, a_{jz})^T$ represent the coordinates of the two vertices for the triangle edge. The position vector p given by equation (10) also has three components:

$$\begin{aligned}
p_x(t) &= p_{0x}(t_k) - \Big(\frac{m}{k_f}\overline{d_{px}^k}\Big)t + \frac{m}{k_f}\Big(\frac{m}{k_f}\overline{d_{px}^k} + v_x(t_k)\Big)\Big\{\exp(tk_f/m) - 1\Big\},\\
p_y(t) &= p_{0y}(t_k) - \Big(\frac{m}{k_f}\overline{d_{py}^k}\Big)t + \frac{m}{k_f}\Big(\frac{m}{k_f}\overline{d_{py}^k} + v_y(t_k)\Big)\Big\{\exp(tk_f/m) - 1\Big\},\\
p_z(t) &= p_{0z}(t_k) - \Big(\frac{m}{k_f}\overline{d_{pz}^k}\Big)t + \frac{m}{k_f}\Big(\frac{m}{k_f}\overline{d_{pz}^k} + v_z(t_k)\Big)\Big\{\exp(tk_f/m) - 1\Big\},
\end{aligned}$$

where $(p_{0x}(t_k), p_{0y}(t_k), p_{0z}(t_k))^T$, $(v_x(t_k), v_y(t_k), v_z(t_k))^T$ and $\left(d_{px}^k, d_{py}^k, d_{pz}^k\right)^T$ are, respectively, the initial position, initial velocity and direction of droplet movement for the k^{th} triangle. We now determine the intersection point (if it exists) between $p(t)$ and each of the triangle edge vectors using Newton's method. Define the three coordinate functions:

$$\begin{aligned} f_1(t,\tau) &= p_x(t) - \ell_x(\tau) = 0, \\ f_2(t,\tau) &= p_y(t) - \ell_y(\tau) = 0, \\ f_3(t,\tau) &= p_z(t) - \ell_z(\tau) = 0, \end{aligned}$$

as functions of the independent variables t and τ. Together, we then have a system of three nonlinear equations that must be solved for t and τ. Here the Newton method has been applied to the reduced system $F(t,\tau) = 0$ where $F = (f_1, f_2)^T$; f_3 is used to validate the solution. At each iteration, t^n and τ^n are updated according to Newton's method as $t^{n+1} = t^n + \delta t, \tau^{n+1} = \tau^n + \delta\tau$, where $(\delta t, \delta\tau)^T = -J_F^{-1}(t^n, \tau^n)F(t^n, \tau^n)$, and $J_F(t,\tau)$ is the Jacobian matrix of F. The iterations are terminated once $\|F^{n+1}\|_2 \leq \tau_r\|F^0\|_2 + \tau_a$. For all of the droplet simulations performed here we have used the initial approximations $t = 0.1$ and $\tau = 0.5$; the relative tolerance was chosen as $\tau_r = 10^{-8}$ and the absolute tolerance was $\tau_a = 10^{-7}$. These parameters provided convergence within eight iterations in most cases. We systematically solve this nonlinear system for each triangle edge until the intersection point is found. This intersection point must satisfy the physical requirement that $t > 0$ and $0 \leq \tau \leq 1$. If this does not occur, or Newton's method fails to converge, we proceed to the next edge and repeat the iterative process. Note that, the point with the minimum time t among all of the intersection points is chosen as t_f.

Once the intersection point is located via the converged solution $(t_f, \tau_f)^T$, the droplet path using equation (10) can be traced across the k^{th} triangle by gradually incrementing t_k until t_d is reached. In order to proceed to the next triangle we move slightly past the intersection point by allowing t_k to be incremented to just beyond t_d. Then, the Matlab command `tsearch` was used to identify the new triangle into which the droplet moves. If no such triangle can be located, the droplet is deemed to have left the leaf surface.

As mentioned before, the droplet has an initial velocity $v_0(t_k)$ from equation (9) when it moves along the leaf surface from one triangle to another. To ensure the droplet is adhered to the surface we project this velocity onto the surface in the direction of movement using $\widetilde{v}_0 = (v_0 \cdot d_p)d_p = v_0 - (v_0 \cdot N)N$,

where N is the unit normal vector given in equation (2). Moreover, this initial speed is updated when the droplet arrives at the next element.

The procedure for simulating the droplet flow on the surface is summarised in the following algorithm:

Algorithm 1. Simulating the Flow of Droplet on a Leaf Surface

INPUT: Mesh of triangles (virtual leaf surface), initial position p_0, initial velocity v_0, initial time t_0, degree of affinity α, friction coefficient k_f and gravity force $F_g = -(0, 0, 9.8)^T$.

Step 1. Place the droplet at some specified point on the leaf surface.
Step 2. Initialize the transit time of the droplet, which is accumulated as the droplet moves from one triangle to another.
Step 3. Determine the triangle in which the droplet is placed using the Matlab command `tsearch`.
Step 4. Determine the direction of movement d_p^k using equation (1) for the k^{th} triangle.
Step 5. Compute the velocity equation (9) of the droplet and then the displacement equation (10) of the droplet at the time t_k.
Step 6. Calculate the transit time t_f required for the droplet to move to the next triangle by intersecting the displacement equation with each side of the triangle edges using Newton's method.
Step 7. Discretise the time interval $[t_k, t_k + t_f]$ using $\Delta t = t_f/N_t$; $t_d = t_k + i\Delta t$, $i = 1, \cdots, N_t$
Step 8. Find the location of the droplet front $x_N(t_d)$ in the k^{th} triangle using equation (7).
Step 9. Evaluate the height of the thin-film h by substituting $x_N(t_d)$ in equation (6).
Step 10. Move the droplet to the next triangle, provided the transit time is less than the time frame and the height of the thin-film $h > \epsilon$.
Step 11. Update the accumulative time, calculate the initial velocity and the new position of the droplet at $t = t_k + t_f$ using steps 6 and 7.
Step 12. Locate the triangle to which the droplet now moves.
Step 13. Repeat steps 4 through 12 for the duration of the animation or until the droplet falls from the leaf surface.

5. Experimental procedure

To illustrate the power of this simple droplet modelling approach, and also to validate the model, a series of water droplet experiments were performed on a freshly cut Frangipani leaf. Initially, six artificial dots were marked on the leaf surface (see figure 4(c)) so that they were clearly visible on all captured images. These six points were used as reference points for the

droplet movement on the leaf surface. The sonic digitizer device shown in figure 4(d) was used to measure the locations of these six points along with the series of leaf boundary points including the end points of the vein depicted in figure 5(a,b). The sonic digitiser used here was a model GP 12-XL, which is nowadays known as Freepoint 3D [22]. This device was manufactured by the Science Accessories Division of the GTCO Corporation (GTCO Calcomp); for further details see [22]. This device captures the x-, y- and z-coordinates of each data point relative to a defined frame of reference in a data file stored on the acquisition computer. Four additional data points on the string attached to the clamp holding the leaf were also recorded. These points were used to determine the direction of gravity with respect to the reference plane of the leaf surface, because the string is assumed to be aligned with the direction of the z-axis (refer figures 4(a) and 5(a)). A syringe was used to measure the droplet mass and two different masses of 0.1 and 0.2 grams were used in our experiment. A video camera recorded the path that the droplet traversed on the leaf surface and the transit time of the droplet also was recorded.

Two different leaf orientations were chosen to simulate the droplet movement shown in figures 4(a,b) and 5(a,b). The second orientation was chosen at a steeper angle than the first. The droplet of mass 0.2 grams was used for the first orientation while the droplet of mass 0.1 grams was used for the second orientation. In fact, the experiment showed that the droplet of mass of 0.1 grams moves very slowly, and in some instances does not move on the leaf surface for the first orientation because the leaf was positioned very close to horizontal. The same sized droplet does, however, move on the surface of the second orientation. The purpose of choosing two different orientations was to test if the droplet path would change if the orientation was altered.

The laser scanner was used to capture the leaf surface points shown in figure 5(c) for the reconstruction of the virtual leaf surface. It was then necessary to transform this more detailed leaf data point set with the points recorded by the sonic digitizer shown in figure 5(a,b). This transformation process required that the laser scanner data points shown in figure 5(c) be rotated to bring them in line with the leaf position that we have in the experiment (again refer to figure 5(a,b)). We now outline the steps carried out to achieve this transformation, where we now refer to the set of data points that were captured using the sonic digitizer as data set 1 and the set of data points that were captured using the laser scanner as data set 2.

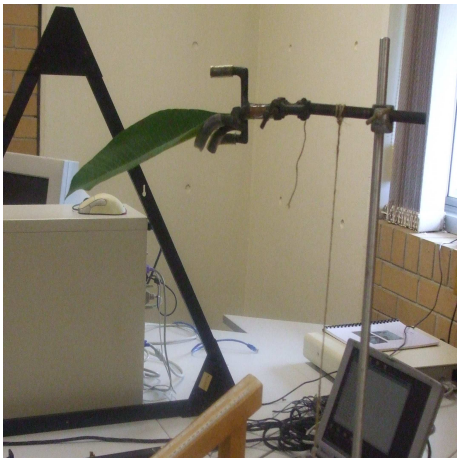

(a)

(b)

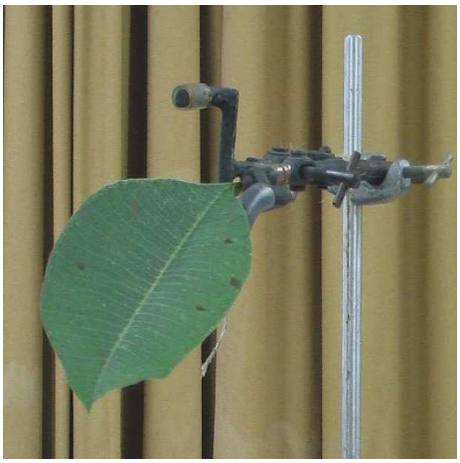

(c)

(d)

Figure 4: (a) exhibits the first orientation of the leaf, (b) shows the second orientation of the leaf, (c) shows the six dots captured using the sonic digitizer and (d) depicts the sonic digitizer device.

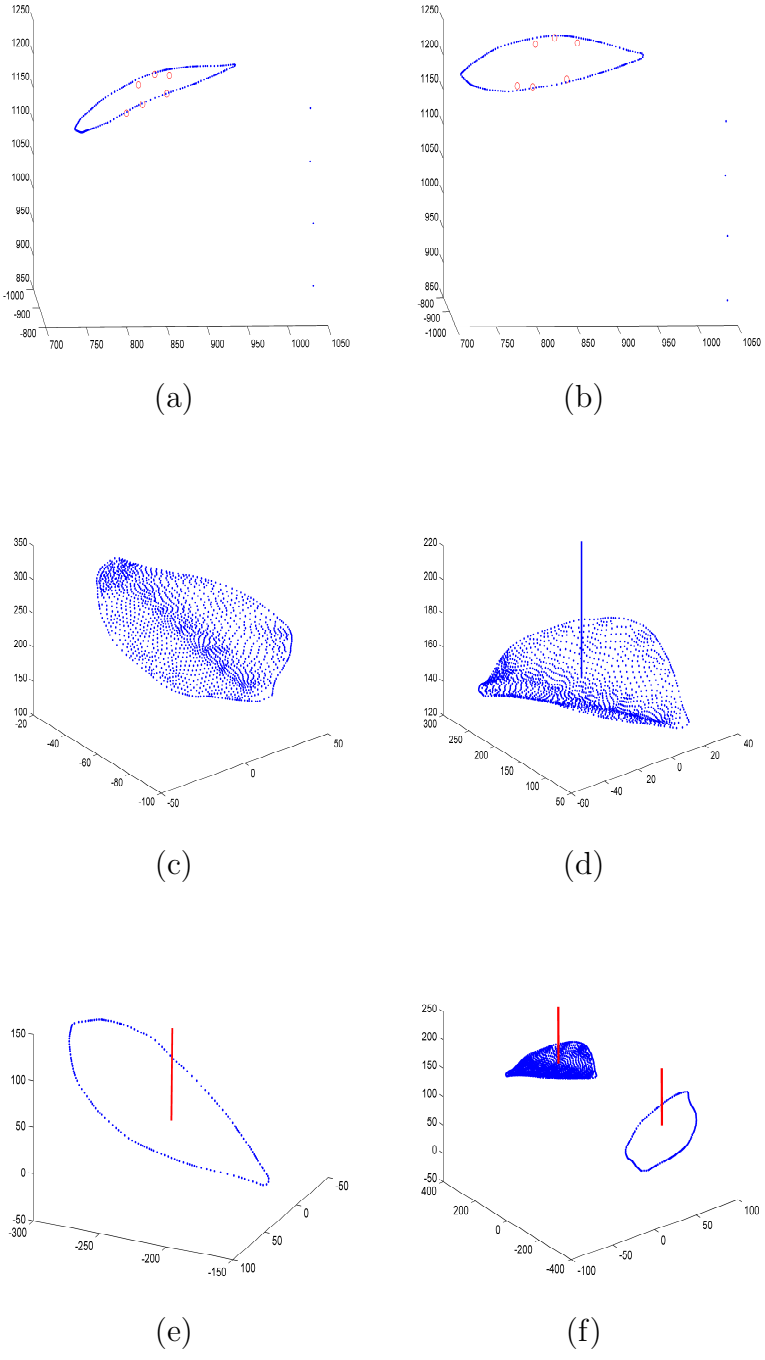

Figure 5: (a) shows the boundary points of the leaf, the string points and the six dots for the first orientation; (b) shows the the second orientation of the data; (c) shows the leaf surface points that were captured using the scanner; (d) depicts the leaf surface points after rotation to the reference plane and its normal; (e) exhibits the sonic digitizer leaf boundary points after rotation to the reference plane and its normal; (f) shows both data sets in the same reference plane.

Transformation Process

1. Determine the reference plane for each data set using the strategy outlined in §3.1 (see figures 5(d,e)). Rotate the axes such that the z-axis is perpendicular to the reference plane as outlined in §3.1 for both data sets (see figure 5(f)).
2. Find the minimum z for each data set and subtract it from the z values such that each set has zero as the minimum point, shown in figure 6(a).
3. The end points of both data sets (the leaf tail) represented by the circle points shown in figure 6(a) were used to bring both data sets together. If $(x_p, y_p)^T$ is the coordinate of one end of the vein of the leaf, change the origin such that $(0, 0)^T$ becomes the end point of the leaf vein.
4. Project both sets of points onto the xy-plane as shown in figure 6(c). Measure the angle between the veins and then rotate the axis so that the veins coincide.
5. Scale the x, y and z coordinates such that the two images coincide as exhibited in figure 6(d).

These transformations are all reversible; they may be applied to the coordinates of the vertical string so that the direction of the gravitational field can be expressed in either set of reference plane coordinates.

After the final representation of the leaf data set has been produced, we started simulating the droplet movement on the virtual leaf surfaces. All of our simulations were performed in Matlab version 7.4 on a 3 GHz pentium 4 processor. The triangulations shown in figures 10(c) and (d) have been used for these simulations. Our model, as we can see from figures 7-9(b,d,f), captured the motion of the droplet on the surface quite well when compared to the motions that were produced in the experiments shown in figures 7-9(a,c,e). We remark that although the viewing angle is slightly different between the experimental and simulation results, this is the best viewpoint chosen from the perspective of the data visualization software. Overall it appears that the simulation results exhibit close to linear behaviour for the flow paths, except near the leaf vein. In the experiments, however, it can be seen that the droplet paths were slightly curved. Figure 7 shows the experimental results compared with the droplet simulations for the first leaf orientation. Observe in figure 7 (a-b) that when the droplet was initially positioned on the lower side of the leaf that the droplet moved parallel to the leaf vein because the external force due to gravity dominated the internal forces on the droplet. However, in 7 (c-d) when the droplet is positioned on

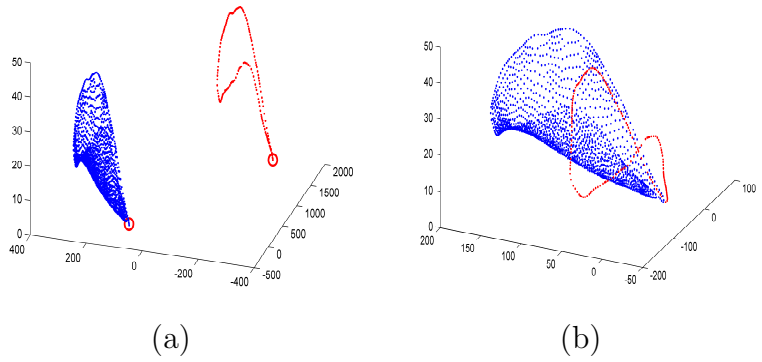

(a)

(b)

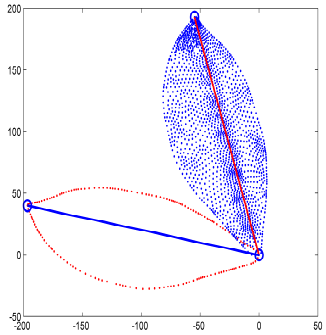

(c)

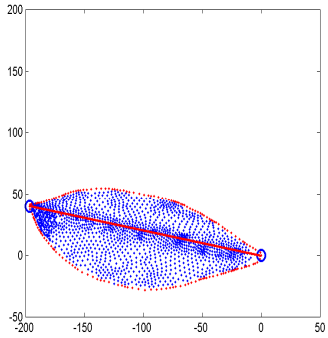

(d)

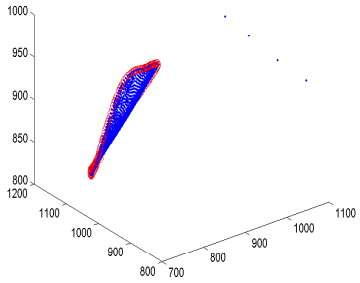

(e)

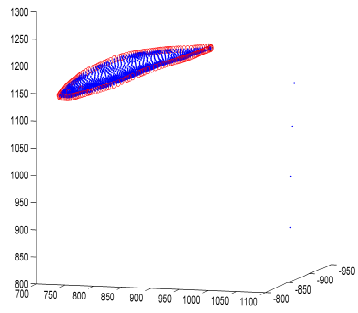

(f)

Figure 6: (a) and (b) show the transformation of both data sets into the $xy-$plane; (c) is the projection of both data sets into the $xy-$plane; (d) is the rotation of the data to become coincident; (e) depicts the inverse rotation of both data sets into the original position that we have in the experiment, where data set 1 is represented by circles while data set 2 is represented by dots; (f) exhibits the final rotation of the first orientation data set and the string.

the high side of the leaf it moves across the surface until reaching the leaf vein, at which stage it continued to move along the vein due to its surface characteristics being conducive to flow. The behaviour of the droplet in figure 7(e-f) is similar to that shown in figure 7(a-b), however in this case the droplet was close to the leaf edge and, as expected, eventually fell from the surface.

The situation is somewhat different for the second orientation exhibited in figure 8, which is positioned much steeper than the first orientation. In particular, we focus on the behaviour of the droplet depicted in figures 8(a-b) and 8(c-d). When the droplet is placed near the upper edge of the leaf, refer to figure 8(a-b) we can see that the velocity of the droplet is large enough to enable it to pass over the vein and continue across the surface until it reaches the lower edge of the leaf, at which time it falls from the surface. However, in figure 8(c-d) the droplet velocity is not large enough to enable it to immediately pass over the vein. Instead, it meanders along the vein before the gravitational force pulls it to leave the vein and continue moving towards the lower edge of the leaf.

One notes from figure 7(c) that when the leaf orientation is close to horizontal that the droplet, after reaching the leaf vein, continues to move along the vein. A plausible explanation for this is that the leaf vein has properties different to the leaf surface properties and this has an impact on the droplet velocity. In order to capture this movement along the leaf vein, we have modified the velocity in our model when the droplet reaches this vein to be a linear combination of the droplet velocity v_0 when it reached the vein, together with an imposed velocity v_n resolved along the vein as (see vein and path shown in figure 7(d))

$$v_{\text{vein}} = \alpha v_0 + \beta v_n, \tag{11}$$

where $0 < \alpha < 1$ and $\beta = 1/\|v_0\|$. Another approach to capture the movement along the vein is achieved by decreasing the surface tension and the resistance of the droplet along this vein.

The procedure we used for simulating the droplet flow along the leaf vein is summarised in the following algorithm:

Algorithm 2. Simulating the flow of a droplet along the leaf vein

Step 1. Find the data points along the vein that coincide with the triangle vertices.
Step 2. Find the triangle that the droplet will move into.

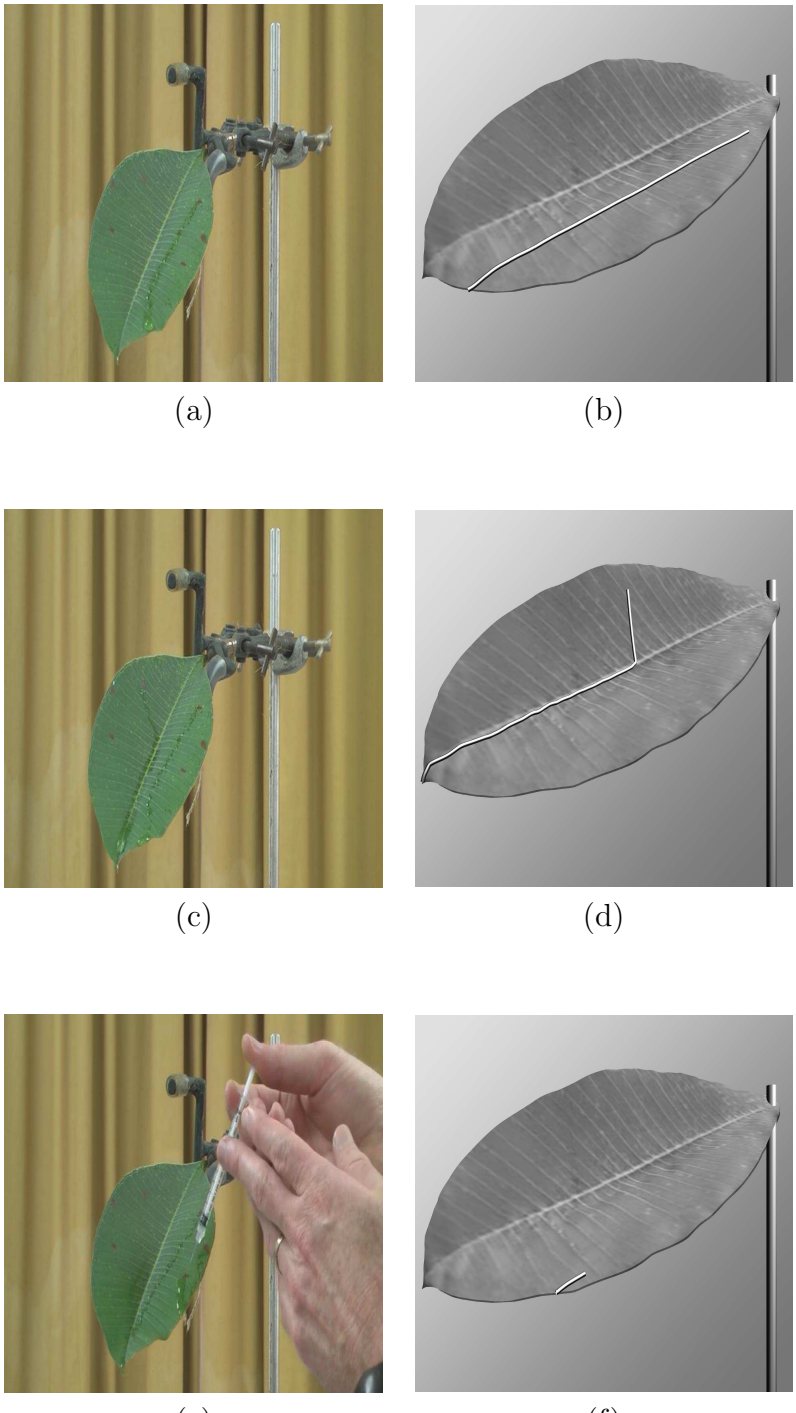

Figure 7: (a,c,e) show the droplet movement across the leaf surface from three different starting positions for the first orientation. (b,d,f) exhibit the corresponding droplet movement generated by the model for the three different starting locations shown in (a,c,e).

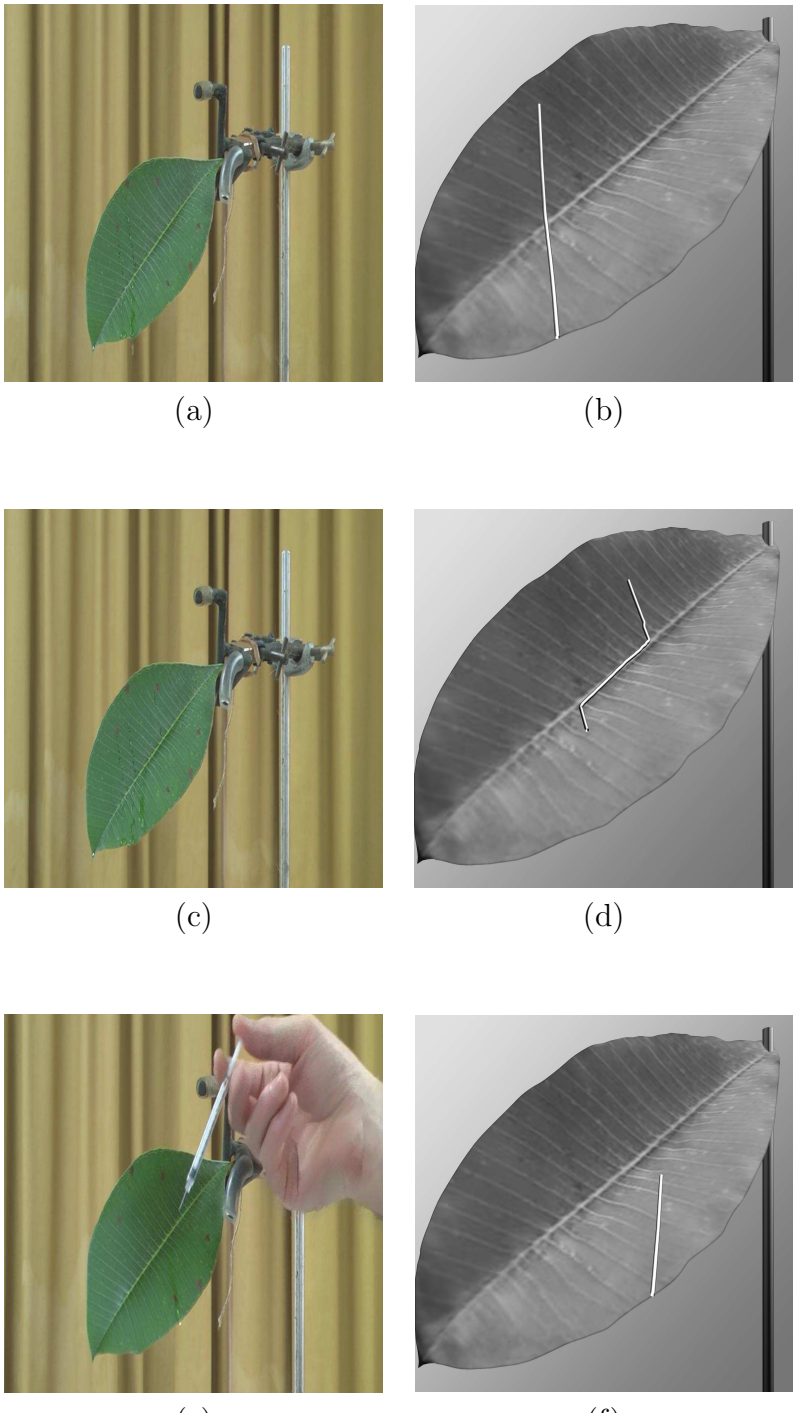

Figure 8: (a,c,e) show the droplet movement across the leaf surface from three different starting positions for the second orientation. (b,d,f) exhibit the corresponding droplet movement generated by the model for the three different starting locations shown in (a,c,e).

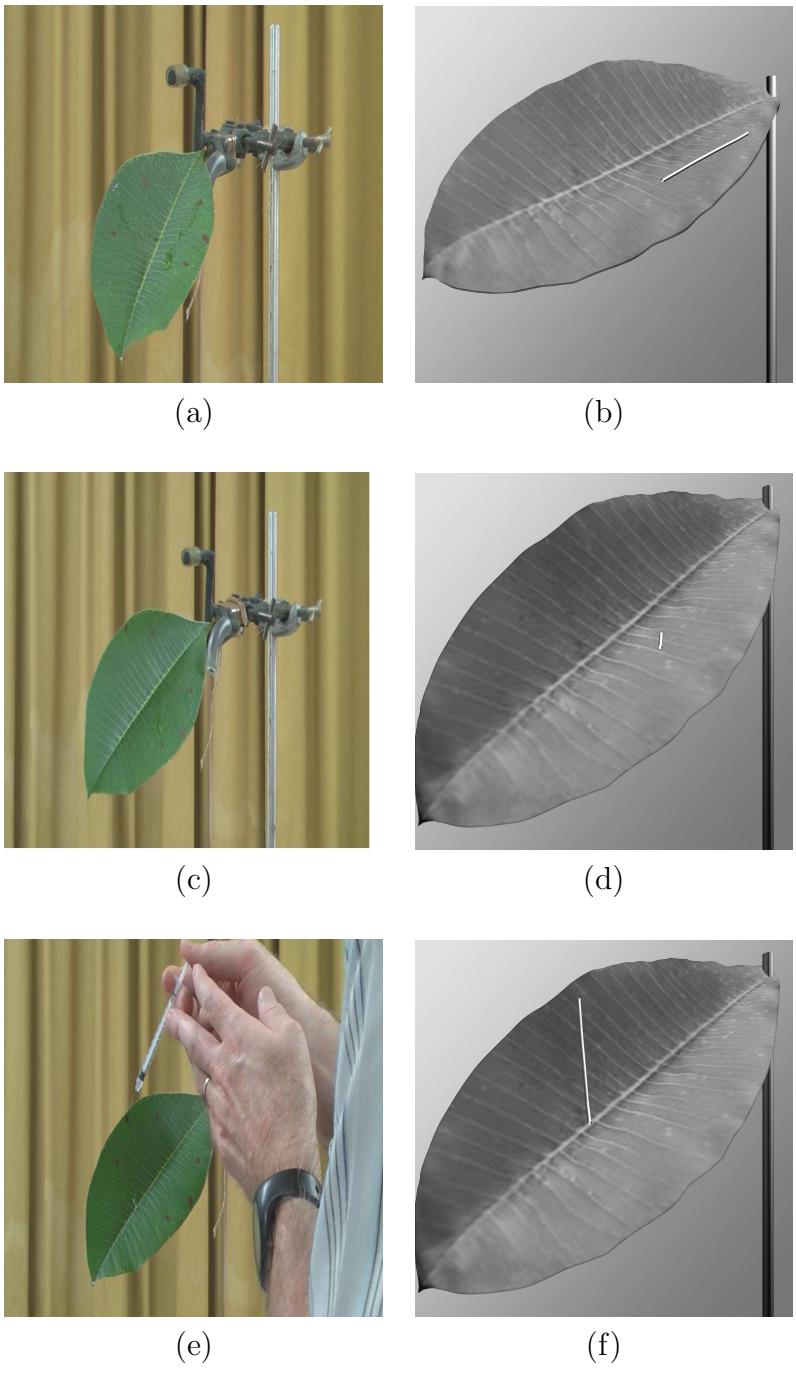

Figure 9: The figures show a comparison of the thin-film model results against the experimental data.

Step 3. Determine if this triangle has any points in common with the vein points.

Step 4. If it has common points, update the velocity to be a linear combination of the droplet velocity when it reaches the vein together with some imposed velocity v_n resolved as shown in equation (11). Otherwise, do not modify the velocity and continue.

The result of applying this algorithm to both leaf orientations can be seen in figures 7(d) and 8(d). One observes from these figures that the droplet motion is more realistic once it reaches and continues along the vein. Without applying this algorithm, the droplet would cross the vein and continue moving until it reaches the leaf boundary, which represents unrealistic droplet motion.

As mentioned above, the droplet starts to move down the inclined leaf surface, and eventually stops at some stage. Figures 9(b,d,f) show comparisons of the droplet movement of our model against the experiments shown in figures 9(a,c,e). By controlling the height of the thin-film in our model we obtained similar movements to the those depicted in the experiments.

To test if the droplet movement is affected by the triangulation of the leaf surface, we have refined the triangulation in both orientations by dividing each triangle into three subtriangles that have their common vertex the centroid of the divided triangle as shown in the figures 10(e,f). Figure 11 shows two paths of the same droplet plotted on the refined triangulation. One path is computed on the unrefined triangulation, given in figures 10 (c,d), while the other path is computed on the refined triangulation, given in figures 10 (e,f). It can be observed from this figure that the droplet paths using the unrefined and refined triangulations are indistinguishable and clearly the droplet motion appears unaffected by the mesh refinement, offering very little change in the direction of movement. We conclude that the motion of the droplet on this particular leaf appears unaffected by refining the triangulation and therefore the coarser resolution can be used to produce acceptable results. This is an important finding because using a refined grid is more computationally demanding.

As mentioned in §4.1, the droplet model contains some parameters such as friction and the resistance coefficient that can be used for calibration. By changing these parameters we can control the droplet movement, or simulate the motion of a pesticide droplet, or nutrient droplet. These movements can be controlled also by changing the height of the thin-film discussed in §4.2. These ideas will be pursued in future research.

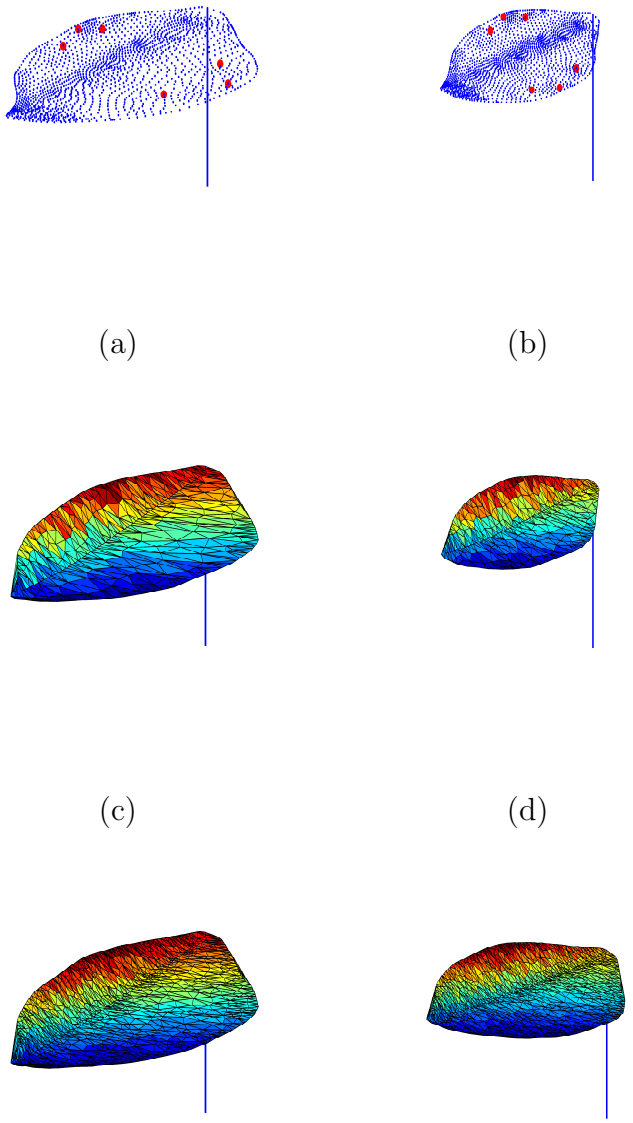

Figure 10: (a) and (b) exhibit the six dots on the final transformed first and second orientation data sets; (c) and (e) represent the triangulation and the refined triangulation respectively of the first orientation data set; (d) and (f) represent the triangulation and the refined triangulation respectively of the second orientation data set.

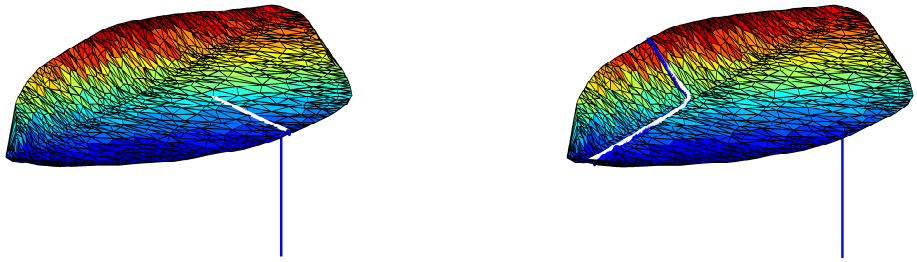

(a) (b)

(c) (d)

Figure 11: Each of these figures show two paths of the same droplet on the refined triangulation. One represents the path on the unrefined triangulation, given in figures 10 (c,d), while the other represents the path on the refined triangulation, given in figures 10 (e,f).

6. Conclusions and future research

The work presented in this paper describes a model for a water droplet moving down a leaf surface. The flexibility of the model offers the user an understanding of how a droplet moves on a leaf surface and how small changes in the dominating factors produce different droplet motions. A new idea based on using thin-film theory has been used to develop a stopping criterion for the droplet as it moves on the surface. Overall the model produces a good representation of the droplet behaviour.

The research described here provides a basis on which future studies can be built. For example, the model may be extended to generate not only realistic movements of a droplet on the leaf surface, but it can also be extended to produce a more physically correct simulation by involving more of the dominating factors and forces that affect the droplet movement. The differences in the nature of leaf surfaces can be included in the model by studying the behaviour of the droplet movement on different leaf surfaces. It can be also extended to study the paths of many droplets of not only water, but also droplets of pesticide moving and colliding on the surface. Knowledge of this path is important for many applications, such as the simulation of a pesticide application to plant surfaces [12, 32]. In the future the model may be used to determine the effectiveness of a treatment, and then to develop certain pesticides that have the ability to protect leaves for longer periods of time. Similar models may treat moisture precipitation and energy uptake through photosynthesis enabled by ray tracing techniques.

Future work will also see the development of more realistic mathematical models for the spreading and sliding of liquid drops on inclined leaf surfaces.

Wetting effects, merging, spraying and adhesion of the droplets has not been implemented in this model. We can include these phenomena by including some of the dominating parameters. Spraying and adhesion could be also included based on the work presented in [6, 7, 36].

7. Acknowledgments

This paper was carried out thanks Mark Barry and Mark Dwyer from the Queensland University of Technology HPC centre for many helpful discussions concerning the droplet visualizations shown in figures 7(b,d,f), 8(b,d,f) and 9(b,d,f). We also acknowledge Dr Jim Hanan from University of Queensland for allowing the use of the equipment to perform the droplet exper-

iments. Finally, we acknowledge the insightful comments of the reviewers that have improved the presentation of the paper.

Figure Captions

- figure 1: The direction of movement d_p with normal N and gravity f^{ext}.
- figure 2: Thin-film flow down a slope.
- figure 3: The droplet movement within the k^{th} triangle.
- figure 4: (a) exhibits the first orientation of the leaf, (b) shows the second orientation of the leaf, (c) shows the six dots captured using the sonic digitizer and (d) depicts the sonic digitizer device.
- figure 5: (a) shows the boundary points of the leaf, the string points and the six dots for the first orientation; (b) shows the the second orientation of the data; (c) shows the leaf surface points that were captured using the scanner; (d) depicts the leaf surface points after rotation to the reference plane and its normal; (e) exhibits the sonic digitizer points after rotation to the reference plane and its normal; (f) shows both data sets in the same reference plane.
- figure 6: (a) and (b) show the transformation of both data sets into the $xy-$plane; (c) is the projection of both data sets into the $xy-$plane; (d) is the rotation of the data to become coincident; (e) depicts the inverse rotation of both data sets into the original position that we have in the experiment, where data set 1 is represented by circles while data set 2 is represented by dots; (f) exhibits the final rotation of the first orientation data set and the string.
- figure 7: (a) and (b) exhibit the six dots on the final transformed first and second orientation data sets; (c) and (e) represent the triangulation and the refined triangulation respectively of the first orientation data set; (d) and (f) represent the triangulation and the refined triangulation respectively of the second orientation data set.
- figure 8: (a,c,e) show the droplet movement across the leaf surface from three different starting positions for the second orientation. (b,d,f) exhibit the corresponding droplet movement generated by the model for the three different starting locations shown in (a,c,e).

- figure 9: (a,c,e) show the droplet movements across the leaf surface from three different starting positions for the second orientation. (b,d,f) exhibit the corresponding droplet movements generated by the model for the three different starting location shown in (a,c,e).
- figure 10: The figures show a comparison of the thin-film model results against the experimental data.
- figure 11: Each of these figures show two paths of the same droplet on the refined triangulation. One represents the path on the unrefined triangulation while the other represents the path on the refined triangulation.

Footnotes

Corresponding author: i.turner@qut.edu.au, Tel.: +61 7 3138 2152, Fax:+61 7 3138 1508.

Email addresses: m.oqielat@student.qut.edu.au (Moa'ath .N. Oqielat), i.turner@qut.edu.au (I.W.Turner), j.belward@qut.edu.au (J.A.Belward), scott.mccue@qut.edu.a (S.W McCue)

References

[1] D.J. Acheson, Elementary Fluid Dynamics, Oxford University Press, United States, 1990.

[2] G.K. Batchelor, An Introduction to Fluid Dynamics, Cambridge University Press, London, 1967.

[3] Q. Chen, Water animation with disturbance model, IEEE Computer Society, USA, 2001.

[4] R. W. Clough, J. L. Tocher, Finite element stiffness matrices for analysis of plate bending, In Proceedings of the Conference on Matrix Methods in Structural Mechanics, Wright-Patterson A.F.B., Ohio, 515-545, (1965).

[5] D. Enright, S. Marschner, R. Fedkiw, Animation and rendering of complex water surfaces, In Proc. of ACM GRAPHITE 02, 736-744, (2002).

[6] W. Forster, J. Zabkiewicz, M. Kimberley, A Universal Spray Droplet Adhesion Model, Transactions of the ASAE, **48**, 1321-1330, (2005).

[7] W. Forster, J. Zabkiewicz, M. Riederer, Spray formulation deposit on leaf surfaces and xenobiotic mass uptake, Proc 7th Internat Symposium on Adjuvants for Agrochemicals, Document Transformation Technologies, Cape Town, South Africa, 332-338, (2004).

[8] N. Foster, R. Fedkiw, Practical animation of liquids, In Proc. of ACM SIGGRAPH 01, 23-30, (2001).

[9] N. Foster, D. Metaxas, Realistic animation of liquids, Graph Models Image Process, **58**, 471-483, (1996).

[10] P. Fournier, A. Habibi, P. Poulin, Simulating the flow of liquid droplets, Proceedings of Graphics Interface, 133-142, (1998).

[11] A. Fournier, W.T. Reeves, A simple model of ocean waves, In SIGGRAPH 86 Conference Proceedings, 75-84, (1986).

[12] J. Hanan, M. Renton, E. Yorston, Simulating and visualising spray deposition in plant canopies, ACM GRAPHITE 2003, Melbourne, Australia, 259-260, 11-14 February (2003).

[13] R. L. Hardy, Theory and applications of the multiquadric-biharmonic method, Comput. Math. Appl., **19**, 163-208, (1990).

[14] H.E. Huppert, Flow and instability of a viscous current down a slope, Journal of Fluid Mechanics, **300**, 427-429, (1982).

[15] M. Jonsson, Animation of water droplet flow on structured surfaces, In SIGRAD 2002 Conference Proceedings, **9**, 17-22, (2002).

[16] K. Kaneda, T. Kagawa, H. Yamashita, Animation of water droplets on a glass plate, Proceedings of Computer Animation 93, 177-189, (1993).

[17] K. Kaneda, S. Ikeda, H. Yamashita, Animation of water droplets moving down a surface, The Journal of Visualization and Computer Animation, **10**, 15-26, (1999).

[18] K. Kaneda, Y. Zuyama, H. Yamashita, T. Nishita, Animation of water Droplet flow on curved surfaces, Proceedings of Pacific Graphics 96, 50-65, (1996).

[19] L. Kondic, Instabilities in Gravity Driven Flow of Thin Fluid Films, SIAM Review, **45**, 95-115, (2003).

[20] P. Lancaster, K. Salkauskas, Curve, Surface Fitting, An Introduction, London, Orlando, Academic Press, San Diego, 1986.

[21] L. Lanfen, L. Shenghui, T. RuoFeng, D. JinXiang, Water Droplet Morphing Combining Rigid Transformation, ICCS 2005, LNCS 3514, Springer-Verlag Berlin Heidelberg, 671-678, (2005).

[22] B. Loch, Surface Fitting for the Modelling of Plant Leaves, Ph.D. Thesis, University of Queensland, (2004).

[23] F. Losasso, F. Gibou, R. Fedkiw, Simulating water and smoke with an octree data structure, ACM SIGGRAPH, **23**, 457-462, (2004).

[24] T. G. Myers, Thin Films with High Surface Tension, SIAM Review, **40**, 441-462, (1998).

[25] B. Niceno, EasyMesh, www-dinma.univ.trieste.it/nirftc/research/easymesh, (2003).

[26] W.K. Nicholson, Linear Algebra with Applications, PWS Publishing Company, Third Edition, p. 275, 1995.

[27] S. OBrien, L. Schwartz, Theory and Modeling of Thin Film Flows, Encyclopedia of Surface and Colloid Science, 5283-5297, (2002).

[28] M.N. Oqielat, J.A. Belward, I.W. Turner, B.I. Loch, A hybrid Clough-Tocher radial basis function method for modelling leaf surfaces, MODSIM 2007 International Congress on Modelling and Simulation. Modelling and Simulation Society of Australia and New Zealand, 400-406, (2007).

[29] M.N. Oqielat, I.W. Turner, J.A. Belward, A Hybrid Clough-Tocher Method for Surface Fitting with Application to Leaf Data, Applied Mathematical Modelling, 2582-2595, (2009).

[30] D.R. Peachey, Modeling waves and surf, In ACM GRAPHITE 86 Conference Proceedings, 65-74, (1986).

[31] W.T. Reeves, Particle system - A technique for modeling a class of fuzzy objects, ACM Transactions on Graphics, **2**, 91-108, (1983).

[32] D.L. Reichard, J.A. Cooper, M.J. Bukovac, R.D. Fox, Using a videographic system to assess spray droplet impaction and reflection from leaf and artificial surfaces, Pesticide Science, **53**, 291-300, (1998).

[33] S. Rippa, An algorithm for selecting a good value for the parameter c in radial basis function interpolation, Advances in Computational Mathematics, **11**, 193-210, (1999).

[34] R. Tong, K. Kaneda, H. Yamashita, A volumepreserving approach for modeling and animating water flows generated by metaballs, The Visual Computer, **18**, 469-480, (2002).

[35] Y. Yu, H. Jung, H. Cho, A new water droplet model using metaball in the gravitational field, Computer and Graphics, **23**, 213-222, (1999).

[36] J. Zabkiewicz, W. Forster, G. Mercer, Spray adhesion and retention crop:formulation interactions, 11th IUPAC International Congress of Pesticide Chemistry, Port Island, Kobe, Japan, 167, August 6-11 (2006).

[37] S. Sikalo, C. Tropea, E.N Ganic, Impact of droplet onto inclined surfaces, Journal of Colloid and Interface Science **286**, 661-669, (2005).

[38] S.F. Lunkad, V.V. Buwa, K.D.P. Nigam, Numerical simulations of drop impact and spreading on horizontal and inclined surfaces, Chemical Engineering Science **62**, 7214-7224, (2007).

[39] H.-Y. Kim, Z.C. Feng, J.-H. Chun, Instability of a liquid jet emerging from a droplet upon collision with a solid surface, Physics of Fluids, **12**, 531-541, (2000).

[40] S.T. Thoroddsen, J. Sakakibara, Evolution of the fingering pattern of an impacting drop, Physics of Fluids, **10**, 1359-1374, (1998).

[41] R. Rioboo, C. Tropea, M. Marengo, Outcomes from a drop impact on solid surfaces, Atomization and Sprays **11**, 155-165, (2001).

[42] A.L. Yarin, Drop impact dynamics: splashing, spreading, receding, bouncing..., Annual Review of Fluid Mechanics **v.38**, 159-192, (2006).